Journal of Polymer Research (2022) 29:351
https://doi.org/10.1007/s10965-022-03210-3

ORIGINAL PAPER

Polymer functional group impact on the thermo-mechanical properties of polyacrylic acid, polyacrylic amide- poly (vinyl alcohol) nanocomposites reinforced by graphene oxide nanosheets

Athmar K. Al-shammari[1,2] · **Ehssan Al-Bermany**[1]

Received: 24 January 2022 / Accepted: 26 July 2022

Abstract
Graphene properties bring significant attention to enhancing the performance of attractive nanocomposites. This investigation focused on the impact of polymer functional groups. Two polymers with the same backbone chain and different end functional groups, poly (acrylic acid) (PAA) and poly (acrylic amide) (PAAm) reinforced with the graphene oxide (GO) nanosheets. The developed mixing-sonication-acoustic method was successfully fabricated PAA: poly (vinyl alcohol) (PVA): GO and PAAm: PVA: GO nanocomposites films. Fourier transforms infrared (FTIR) revealed the strongly interfacial interaction between polymers and GO nanosheet, supported by shifting in the polymer's X-ray diffraction (XRD) peaks and an increase in the crystallite size of the polymer. Scanning electron microscopy (SEM) exhibited fine homogeneous and good nanomaterials dispersion in the polymers matrix. The sample showed better thermal stability, conductivity, and mechanical properties. The contribution of GO showed a remarkable change in the structure, morphology, differential scanning calorimetry (DSC), and slight enhancement of thermogravimetric analysis (TGA) results up to 25% and 20%, in contrast, thermal conductivity (TC) displayed notable enhancement up to 50% from 10.76 to 16.24 W/m ^{o}C, and 225% from 3.54 to 11.24 W/m ^{o}C, of PAA-PVA/GO and PAAm-PVA/GO nanocomposites, respectively. The mechanical properties such as ultrasound velocity, compressibility, and modulus of elasticity revealed notable enhancement after the contribution of GO up to 85%, 75% and 76%, 81%, and 233%, 148% of PAA-PVA/GO and PAAm-PVA/GO nanocomposites, respectively, compared to their blended polymers. Adsorbed radiation significantly enhanced 24% by acid group nanocomposites and showed promising sensors, thermostats, and other applications.

Keywords Polymers functional groups · PAAm · PAA · GO Nanosheets · Thermomechanical properties

Introduction

High-performance nanocomposites have attracted significant attention from researchers and engineering for wide and new applications. Several factors and challenges faced the researchers to achieve good nanocomposites, for instance, homogeneity, fine nanomaterials dispersion, strong interfacial interaction, load transfer, etc. [1, 2]. Functionalising the materials is an imperative key that could directly impact overcoming these challenges and achieving significant interfacial interaction between nanocomposite components for new and high-performance nanocomposites. The functional groups of polymer and nanofillers are among the most effective factors that could form a strong interfacial interaction between the matrix and nano-fillers. Also, it could achieve a homogenous and stable matrix, assist in good load transfer between the polymer and nanomaterials in the matrix and bring great improvement in achieving [3, 4]. In contrast, the loss of bonding, aggregation, weak interaction, and failure results from the lack of the component's functional groups, which may reduce the nanocomposites' properties. This important factor, the polymer functional group, is not fully understood with a lack of information in this field. Where most of the investigation focused on the functionalisation of the nanofillers only, for instance, graphene [5], silica nanoparticles

✉ Ehssan Al-Bermany
ehssan@itnet.uobabylon.edu.iq

[1] Department of Physics, College of Education for Pure Science, University of Babylon, Babil 51001, Iraq

[2] Educational Directorate of Babylon, Ministry of Education, Babil 51001, Iraq

Published online: 29 July 2022

[6], and nano-SiO_2 [7], to improve the homogeneity of the filler and enhance the compatibility and nanofillers interaction in the polymer matrix. Therefore, the study focused on involving the polymer function group with the graphene oxide nanosheets (GO) function group to reduce the knowledge gap and achieve better interfacial interaction for high-performance nanocomposites using nanotechnology.

Nanotechnology has wide and speared applications in science and technology [8]. Nanomaterials characterisation has different physicochemical properties, such as graphene and its derivatives. Graphene nanosheets' have outstanding mechanical modulus with 1 TPa and breaking strength reaching about 125 GPa [9], high thermal conductivity ~ 5000 W m^{-1} K^{-1}, and high electron mobility of 200 000 cm^2 v^{-1} s^{-1} [10]. Graphene oxide nanosheets (GO) have a large specific surface area of 2630 m^2 g^{-1} and are rich in function groups, such as hydroxyl, carboxyl, epoxy, carbonyl groups, etc. [11, 12]. The functional group turns to GO into strongly hydrophilic nanomaterials that assist to be more capable of uniform distribution, strong interactions with other materials and transfer the loading through the whole materials [13, 14]. Based on that, graphene increases the interfacial strength between the components of the mixture and the other graphene sheets, which plays another role by distributing the forces acting on the material over all parts and dispersing the applied load [15, 16]. Graphene gives more ability for the material to withstand the applied pressure and greater hardness with resistance to shocks [17–19]. These unique properties of graphene gave high potential for producing unique properties and wonder or novel polymer-nanocomposites even at a very low load without affecting the transparency of the materials or polymers [20, 21]. Graphene is a multifunctional wonder material used in different areas and has great adaptability to attract many applications as chemists, drug delivery, environmental, engineering, nano-electronics, sensors, supercapacitors, etc. [4, 22, 23].

This investigation focused on the efficiency of the polymer functional groups instead of nanomaterials functional groups to increase the compatibility of nanocomposite components. Therefore, polymers were selected with the same backbone but with different end functional groups: poly acid (PAA) with the acid group and polyacrylamide (PAAm) with an amide. PAA has a high negative charge density from the carboxylate group of two carbon atoms in the main PAA chain [24]. PAAm is a non-toxic polymer and soluble in water polymer, which is interesting to improve the materials' viscosity, soft contact lenses, oil recovery, flocculants, cover burns tissues, and water mining treatment [25]. In addition, polyvinyl alcohol (PVA) is not toxic, soluble in water, biocompatible, and has good elasticity with a high tensile strength [5, 26]. Moreover, PVA has polarised groups [14, 27] and hydrogen bonds with the hydroxyl groups [4, 28] associated with more compatibility between the nanocomposite components.

J., Chen, et al. (2012) [29] reported an improvement in the thermal stability and efficacy of 1,3-bis(2-chloroethyl)-1-nitrosourea (BCNU) with glioma cells applying the PAA functionalised cellular concentration. Covalently bound to the nanocarrier increases the cancer cells' effective absorption of PAA-GO. The In-vitro anticancer efficacy improved by up to 30% within the DNA and crosslinking of PAA-GO-BCNU and a 77% reduction in the IC 50 value for GL 261 cancer cells compared with the same free-BCNU dosage. Osma et al. [30] investigated increasing the temperature impact and GO nanosheets on the swelling of the PAAm-GO composite. Cooperative diffusion coefficients were calculated using Li Tanaka's model supplemented with Stern Volmer's Equations. GO may work as a multifunctional cross-linker, forming more PAAm-GO composite junctions, increasing crosslink density, and lowering swelling power. Li et al. [31] study the shape memory polymers of dispersing PAA-GO into the PVA mixture. They create a PVA/PAA-GO with 3% films for thermal and near-Infrared light brought shape memory. This study combines high mechanical strength with the capacity to rebuild the mechanical damage with the exhausted form memory of the PAA-GO composites. Reinforced the self-healing PVA/PAA with a 3% loading ratio of GO presented a durable structure, great thermal and near-Infrared light the persuaded shape memory capacity. The fracture stress and Young's module exhibit 70.4 MPa and 2.8 GPa, respectively.

Few investigations [29–31] were carried out on polyacrylacid (PAA) or polyacrylamide (PAAm) with PVA. In contrast, the investigation focused on studying the impact of the function group of polymer with functional groups of graphene oxide nanosheets reinforced the structure and thermo-mechanical properties of nanocomposites.

The experimental part

Materials

Sigma-Aldrich Company, UK, produced graphite powder ($\leq$40 µm) and other materials used to synthesise GO. PVA, Mw, 160,000 g mol^{-1}, was produced by Dindori, Nashik, India, PAAm, Mw, 5–30 million g mol^{-1}, PAAm, Mw, 5–30*10^6 g mol^{-1}, and PAA, Mw, 250,000 g mol^{-1}, were obtained from Shenzhen sendi Biotechnology Co. Ltd, China.

Methods

Synthesis of GO

The synthesis process of GO was illuminated in supplementary information and previous literature [2].

Preparation of samples

The exponential methods flowed in three steps. Firstly, each of the three polymers (PAA, PAAm, and PVA) was dissolved in distilled water (DW) independently at a 49.5 wt. % using a magnetic stirrer for 2 h. Meanwhile, GO was suspended in DW at 1 wt. % with the assistance of magnetic starrier and sonication bath.

Secondly, PAA was mixed with PVA at a ratio of (1:1) as (50: 50 wt. %) for 4 h to prepare blended polymers PAA-PVA, then (1 wt. %) of GO was loaded to the mixture of blended polymers with a ratio of (49.5: 49.5: 1 wt. %) for (PAA: PVA: GO) to get PAA-PVA/ GO nanocomposites. The components were mixed for 30 min, and then the mixture was sonicated using a sonication bath for 15 min. This process was repeated for the first 24 h. Then followed by mixing only without sonication for two weeks using a magnetic stirrer to achieve strong interfacial interaction, homogeneity and good dispersion of the nanomaterials in the polymers matrix. This same process was repeated to prepare the PAAm-PVA and PAAm-PVA/ GO nanocomposites.

Finally, samples were located in a petri dish and left to dry under air for dry, where all the procedures were carried out at room temperature (20 ± 3 °C).

Characterization

Fourier Transforms Infrared (FTIR) type vertex 70 made by Bruker Company, Germany, working between 4000 -500 cm^{-1}, XRD Diffraction type Xpert, Phillips, Holland, and Filed Effect Scanning Electron Microscopy (FESEM) type Mira-3, with 1.2 nm at 30 kV; 2.3 nm at 3 kV, Tescan, France, were applied to characterise the sample structure and morphology. Thermogravimetric-differential scanning calorimetry (TGA/DSC 3 +), Elmer, Agilant, Perkin Elmer, USA, and Lee's Disk manufactured by British Griffin and George were used to record the thermal properties of the samples. Ultrasound velocity multi ultrasound frequency instrument type SV-DH-7A/SVX-7, made in Korea, was used at (45) kHz for recording the ultrasound mechanical properties. In addition, Sr-90, 1 μ CI, 28.6 years with Beta radiations was used for radiation measurement. The source was pleased 3 cm away from the counter (detector of Geiger). Meanwhile, the samples were located (2 cm) away from the radiation source.

Results and discussion

Figure 1 illustrates the FT-IR spectra of the samples. The spectra of PAA-PVA blended polymers showed several peaks at 3292 cm^{-1} of hydroxyl group stretch (O–H), 2940 cm^{-1} of methylene stretch (C-H_2), 1706 cm^{-1} of carboxyl acid stretch (C = O), 1212 cm^{-1} of the hydroxyl group bend (O–H), and 1082 cm^{-1} carbon dioxide stretch (C-O) in agreement with other reports [29, 31, 32]. In contrast, the contribution of GO revealed impacts and shifting of the most peaks, such as form 3292 to 3254, 2940 to 2912, 1706 1700, 1218 to 1212, and 1077 to 1051 cm^{-1} of the spectra of PAA-PVA/ GO nanocomposites compared with PAA-PVA blended polymers. The second blended polymer PAAm-PVA revealed a broadband peak at 3285 cm^{-1} of hydroxyl (O–H) group, 2940 cm^{-1} of (C-H), 1715 cm^{-1} of carboxyl acid (C = O) stretch, 1644 cm^{-1} of the amide group, 1258 cm^{-1} of hydroxyl group, (O–H), and 1087 cm^{-1} of the epoxy group (C–O–C) in agreement with the literature [24, 33]. Whereas the contribution of the GO nanosheets exhibited shifting in the most peak, for instance, 2946 to 2940,

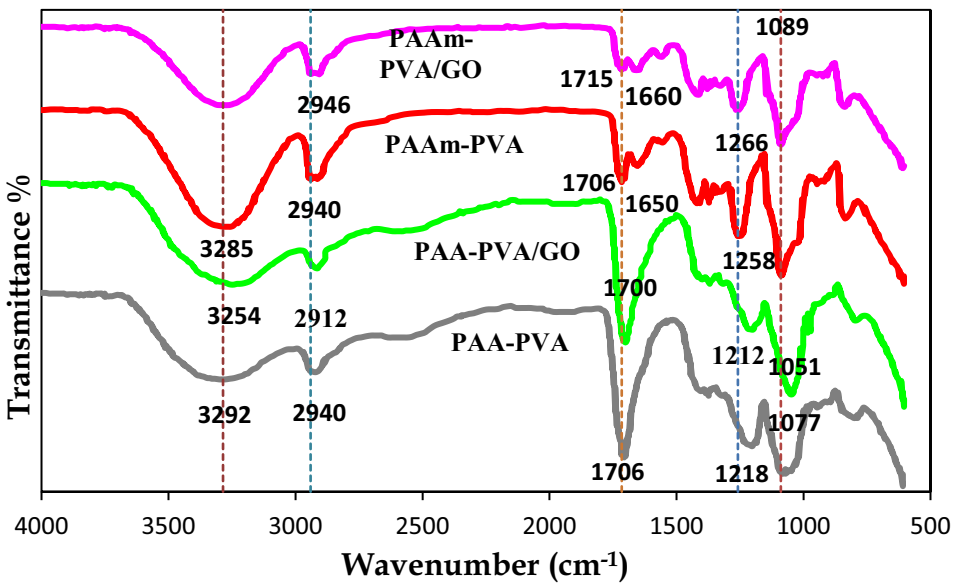

Fig. 1 FTIR spectra of samples

1715 to 1706, 1660 to 1650, and 1266 to 1258 cm^{-1} of the spectra of PAAm-PVA/ GO nanocomposites compared with PAAm-PVA blended polymers, this behaviour agreed with other findings [2, 4, 14].

Both samples showed good formulation of the functional groups of both polymers in the blended polymer samples and the nanocomposites. In contrast, the loading GO nanosheets presented stronger interfacial interaction from the shifting in the position peaks of the functional group that could relate to the formulation of the strong hydrogen interfacial interaction between the functional group of polymer and the GO functional groups in agreement with other researches findings [14, 34, 35].

XRD patterns of both blended polymers and nanocomposites are exhibited in Fig. 2. Interestingly, these blended polymers exhibited a different structure even though they had the same backbone. Where PAA/PVA blended polymer exhibited ten XRD peaks at 2θ = 15.0°, 16.6°, 19.9°, 21.2°, 23.6°, 25.9°, 31.1°, 33.7°, 40.9°, and 42.9°, these related to PAA polymer in agreement with the other reports [36–38], in addition, to the PVA peak at 2θ = 19.9° that matched the literature [4, 39]. In contrast, the contribution of GO in the PAA/PVA-GO nanocomposites revealed significant shifting to 15.2°, 16.9°, 20.0°, 21.4°, 26.3°, 31.4°, 33.9°, 41.2°, and 43.3° compared PAA/PVA blended polymers, in addition to a small feature of the GO peaks at 2θ = 10.6 ° in agreement with the literature [2].

The spectra of PAAm-PVA displayed peaks at 2θ = 32.1°, 45.8°, 56.9°, 66.6°, and 75.7°, which related to PAAm, in agreement with the other findings [34, 40]. In addition, the PAAm-PVA blended polymer exhibitions the small feature of PAAm and the PVA peak at 2θ = 19.9°, in agreement with the literature [41]. The PAAm-PVA/GO nanocomposites revealed small shifts in these peak positions, as shown in Fig. 2. The contribution of GO did not affect the structure of polymers and displayed a slight shift in the peak positions. Moreover, the crystallite size (D) of PAAm-PVA was higher by 24.5% than PAA-PVA. It was significantly increased after the loading of GO up to 57% and 43% of PAA-PVA/GO and PAAm-PVA/GO nanocomposites. The average lattice strain also exhibited a clear influence on the functional group between the polymers and the contribution of GO, which showed another effect in the results.

The peak position estimates the interplanar d-spacing by applying the Bragg equation [42].

$$n\lambda = 2\ d\ sin\ (\theta) \tag{1}$$

where (n), (λ), (d), and (Θ) mean the integer, X-ray wavelength, d-spacing, and angle of X-ray between the incident

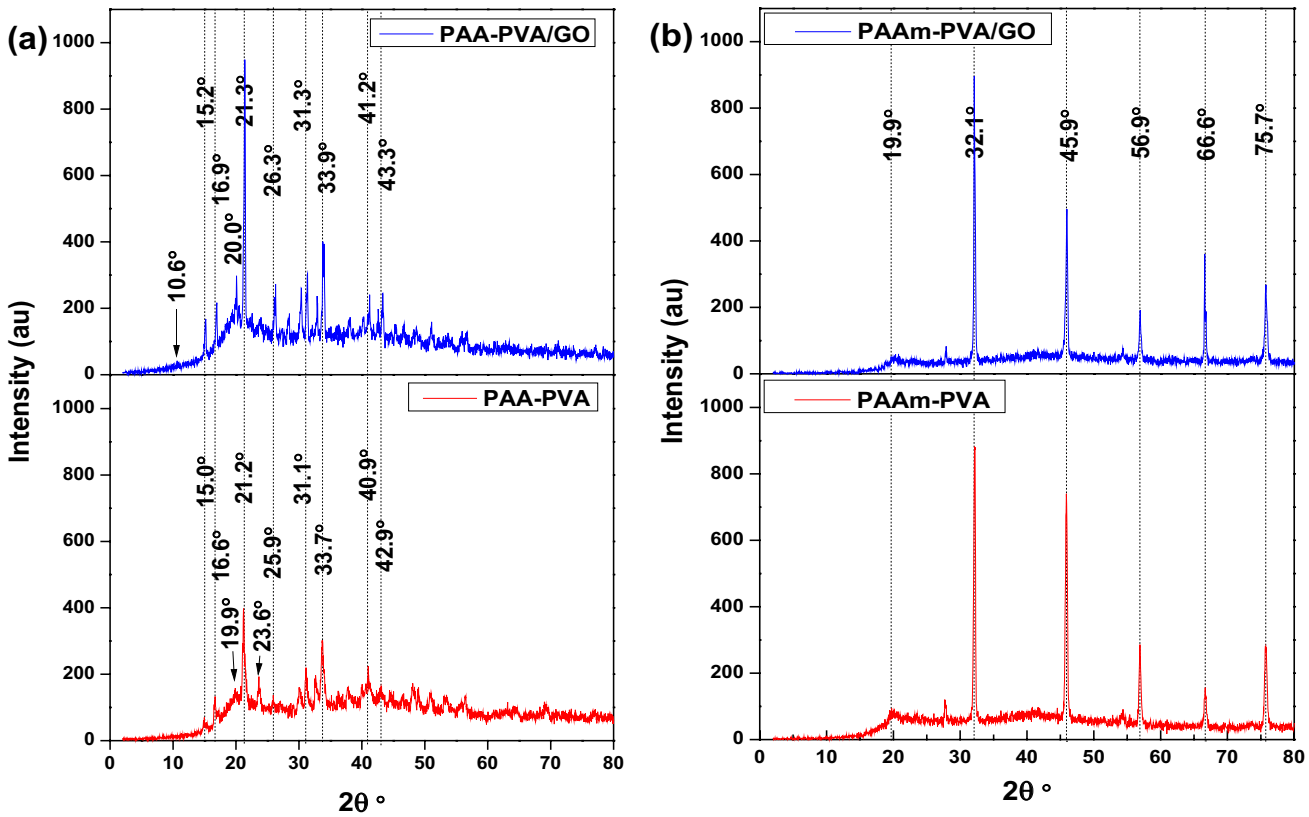

Fig. 2 XRD patterns of samples

and scattering beam, respectively. Whereas the crystallite size (D) in (nm) and lattice strain (ε) were calculated from the Scherrer formula (2), and Eq. (3), respectively [43].

$$D = k\lambda\ /\beta\ \cos\ (\theta) \tag{2}$$

$$\varepsilon = \beta\ /4\ tan\ (\theta) \tag{3}$$

where (k) and (β) mean the form factor of the mean of the crystals, which is equal to ($k = \sim 0.9$), and the full width of the material reaches the peak at half the maximum (FWHM), respectively. The crystallite size was increased of the nanocomposites after the involvement of the GO nanosheets with the blended polymer, as exposed in Table 1.

Figure 3a-f display the FESEM micrograph images of the PAA-PVA blended polymer and PAA-PVA/GO nanocomposite films surface with different magnifications, respectively. The PAA-PVA blended polymer found a uniform shape revealing cracks in the surface, as shown in Fig. 3a, b, and c. These cracks were significantly reduced and disappeared after GO's contribution. PAA-PVA/GO nanocomposite exhibited a more uniform and smoother surface than PAA-PVA, as shown in Fig. 3d, e, and f. This behaviour could relate to the strong interfacial interaction between the polymers and nanographene sheets, as presented in the FTIR results.

In Fig. 3a, b, and c, FESEM images of the PAAm-PVA polymer mixture showed the shape of ice cubes. The addition of the graphene oxide nanosheets into the PAAm-PVA revealed notable changes in the surface and morphology shape of the PAAm-PVA/GO nanocomposite, as illustrated in Fig. 3d, e, and f. Where nanosheets of GO were provided well-distributed clusters without any aggregation, this change could be related to the formulation of the strong interfacial interaction between the functional groups of GO nanosheets with the functional groups of the blended polymer. That exhibited a significant change in the

Table 1 Summarized the diffraction angle, FWHM (β), d-spacing, crystallite size (D), average crystallite size, and the average lattice strain of blended polymers and nanocomposite

Samples	2θ (°)	β (°)	d (nm)	D (nm)	Average crystallite size (nm)	Average lattice strain * 10^{-3}
PAA-PVA	15.00	0.33	0.46	24.28	20.26	8.65
	16.60	0.30	0.51	26.76		
	19.90	0.32	0.48	25.20		
	21.22	0.40	0.38	20.20		
	23.60	0.46	0.33	17.64		
	31.10	0.43	0.36	19.17		
	33.73	0.54	0.28	15.37		
	40.90	0.63	0.24	13.45		
	42.90	0.83	0.19	10.28		
PAA-PVA/GO	15.20	0.29	0.52	27.63	32.60	5.12
	16.90	0.22	0.68	36.50		
	20.00	0.23	0.67	35.07		
	21.30	0.24	0.62	33.68		
	26.30	0.22	0.70	37.08		
	31.33	0.18	0.84	45.83		
	33.90	0.33	0.46	25.16		
	41.20	0.32	0.48	26.52		
	43.30	0.33	0.46	25.90		
PAAm-PVA	32.13	0.31	0.49	26.24	24.50	3.30
	45.88	0.37	0.41	23.20		
	56.90	0.38	0.40	23.76		
	66.67	0.37	0.41	25.68		
	75.73	0.42	0.36	23.61		
PAAm-PVA/GO	32.12	0.27	0.56	30.20	35.05	2.41
	45.93	0.28	0.54	30.61		
	56.92	0.23	0.66	39.06		
	66.63	0.26	0.58	35.87		
	75.77	0.25	0.60	39.53		

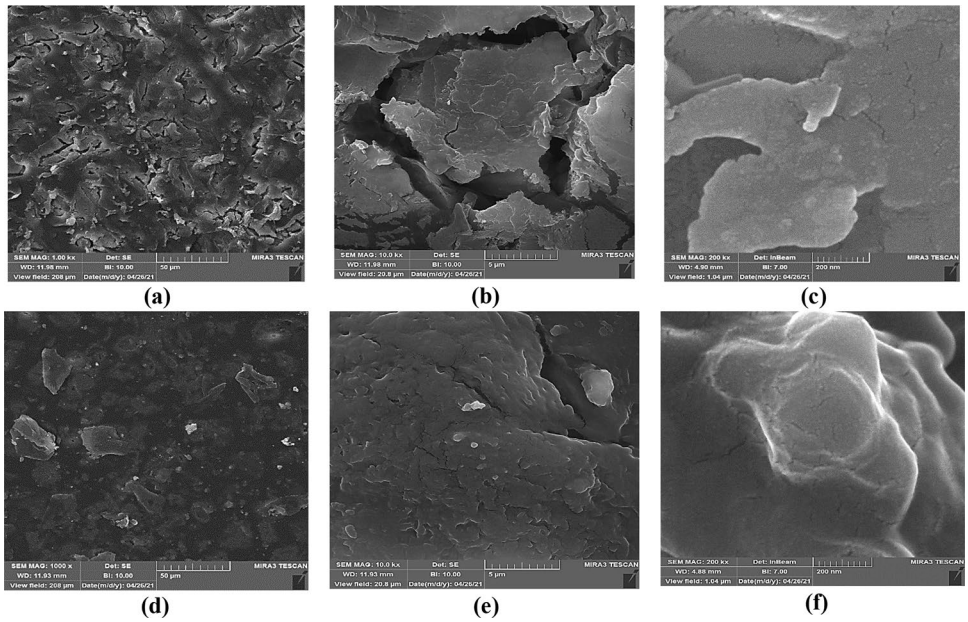

Fig. 3 FESEM images (**a**, **b**, and **c**) of PAA-PVA blended polymers and (**d**, **e**, and **f**) PAA-PVA/GO nanocomposite

nanocomposite morphology and mechanical behaviour. These findings are supported and agree with FTIR, XRD and OM findings.

Figure 4a and b illustrates the TGA curves of sample films. PAA-PVA blended polymers curve showed two segments, as exhibited in Fig. 5a. The main first degradation segment was degraded about 74.4% of the ratio of the sample between 100 to 600 °C. The second degradation segment was degraded by about 8% between 700 to 900 °C. Therefore, only 12.3% remained materials of PAA-PVA at 900 °C. In comparison, PAA-PVA/GO nanocomposites also exhibited two segments. They presented the same behaviour as PAA-PVA. PAA-PVA/GO nanocomposites exposed an enhancement up to 37% at 900 °C in the thermal behaviour compared with PAA-PVA after GO loading, as shown in Fig. 4a. This behaviour was greed, with another finding in literature [34].

In the range between 25 °C to 250 °C, samples with the amide group PAAm-PVA and PAAm-PVA/GO exhibited good thermal stability, as shown in Fig. 4b. It exhibited one segment of degradation in the range between 250 to 600 °C. Then, the thermal behaviour remained steady from 600 to 900 °C. The TGA behaviour of PAAm-PVA exhibited degradation of up to 60%, whereas the PAAm-PVA/GO was

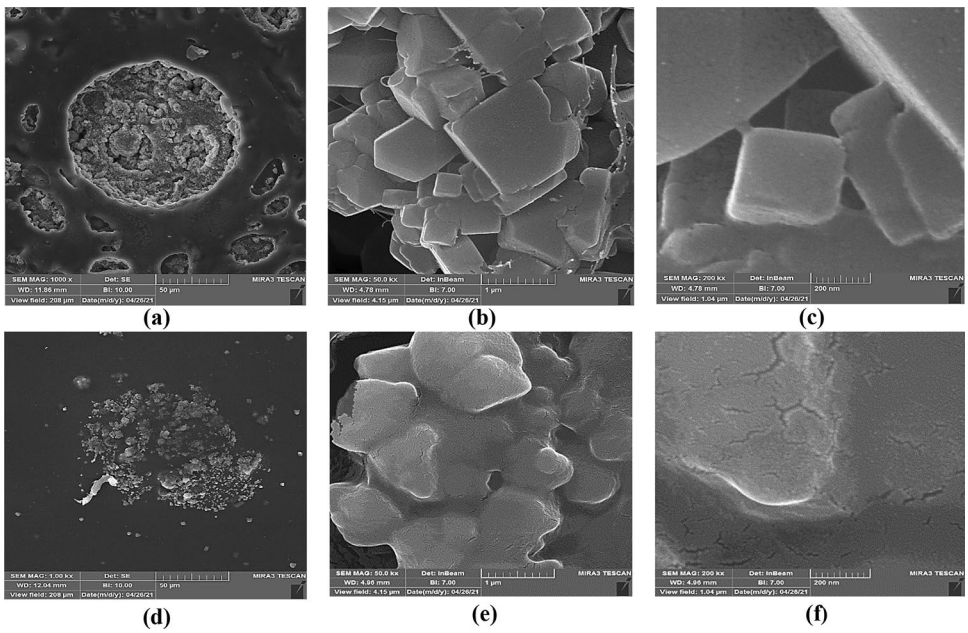

Fig. 4 FESEM images (**a**, **b**, and **c**) PAAm-PVA blended polymers and (**d**, **e**, and **f**) PAAm-PVA/GO nanocomposite

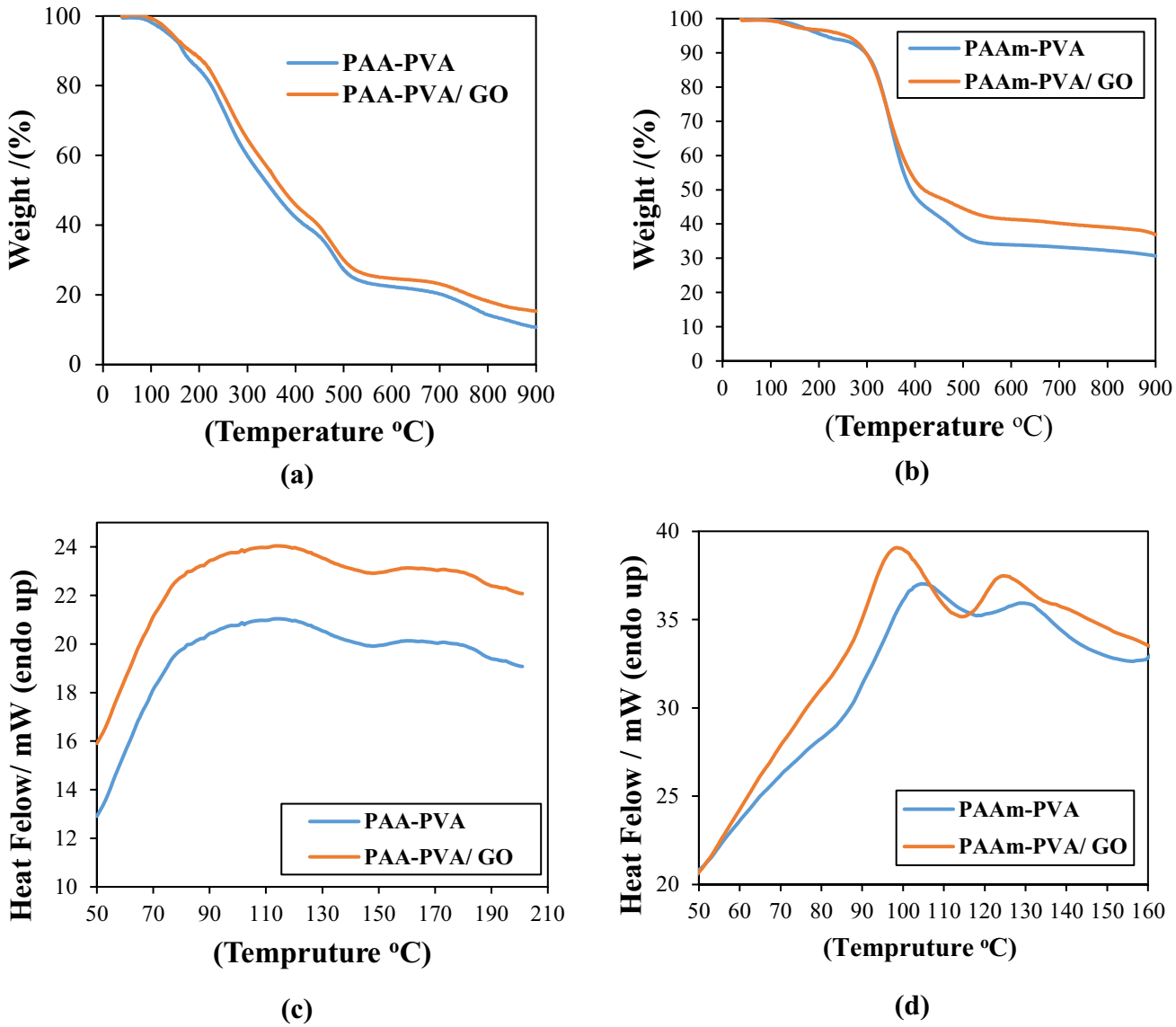

Fig. 5 (**a** and **b**) the thermal gravimetric analysis and (**c** and **d**) the differential scanning calorimetry of the samples

degraded up to 51% between 250 to 600 °C. Generally, at 900 °C, the contribution of GO has slightly improved the thermal stability of PAA-PVA/GO nanocomposites up to 25% compared with PAA-PVA blended polymer.

Extraordinarily, despite both the PAA and PAAm having the same backbone, these samples exhibited a different thermal stability behaviour because it contains a different functional group. The degradation behaviour started earlier at 100 °C of PAA-PVA and PAA-PVA/GO nanocomposites with two segments of degradation. In contrast, PAAm-PVA and PAAm-PVA/GO nanocomposites with amid group started degradation at 250 °C with only one segment, which displayed better thermal behaviour than the sample with the acid group. In addition, thermal behaviour enhanced after the contribution of GO compared with PAA-PVA/GO. This finding agrees with several works of literature that revealed the same thermal stability and degradation behaviour of PAA [23, 29, 44] and PAAm [45, 46] after reinforcing with nanomaterials. Generally, at 900 °C, the contribution of GO has improved the thermal stability of PAAm-PVA/GO nanocomposites slightly up to 25% and 20% of PAAm-PVA. In contrast, GO impacts more on the thermal behaviour of PAAm-PVA revealed than PAA-PVA.

Differential scanning calorimetry (DSC) endothermic and the first-order transition of blended polymers and nanocomposites using the onset are shown in Fig. 4c and d. Figure 4c reveals the melting transition temperature calculated for PAA-PVA. PAA-PVA exhibited two melting transition temperature peaks (T_m) at 118.5 and 175.8 °C [32]. A small reduction of these the melting peak

temperature (T_m) to 115.6 and 175.2 °C, respectively, after GO contribution in the PAA-PVA/GO nanocomposite.

Figure 5d shows the melting transition temperature (T_m) peak of the PAAm-PVA blended polymer at 107 and 133 °C [47]. Also, the reduction in these melting temperatures (T_m) peaks to 100.6 and 126.4 °C, respectively, due to the contribution of GO in the PAAm-PVA/GO nanocomposites. This shifting to the lower value of T_m is associated with the bonded between the blending polymers and GO functionals. This interaction strongly restricted the blended polymer chain's mobility at the interface by GO, giving a reasonable improvement in the thermal and mechanical behaviour [7, 48]. Interestingly, samples with acid groups showed better thermal stability through a lower reduction in the Tm temperature. These results matched the TGA results that showed slight improvement after the contribution of GO.

Lee disk procedure was used to characterise the sample's thermal conductivity before and after loading of the GO. The results of the thermal conductivity were determined by applying Lee's disc apparatus methods [49] from the following Eqs. (4 and 5) [50].

$$\mathrm{I.V} = \pi r^2.\mathrm{e.(T1 + T3)} + 2\pi \mathrm{re[d1.T1} + \frac{1}{2}.\mathrm{ds(T1 + T2)} + \mathrm{d2.T2 + d3.T3]} \quad (4)$$

$$K.\left[\frac{T2 - T1}{ds}\right] = e.[T1 + \frac{2}{r}.\left(d1 + \frac{1}{2}ds\right).T1 + \frac{1}{r}ds.T2] \quad (5)$$

where (I) represents the current passing through the coil of the heater (Amber), and (V) is the potential difference at the two ends of the heater coil (Volt). (r) and (e) represent the disk radius and the heat loss per unit time (seconds) over an area, respectively. T1, T2, and T3 (ºC) were measured during the first, second, and third disks, respectively. d1, d2, and d3 represent the thickness of samples, (ds) means the disc thickness, and (K) refers to the thermal conductivity (W /m. ºC) [50]. The heat loss per unit time (e) was calculated from Eq. (4). Equation 4 measured the difference in temperatures between the disks and their surroundings in addition to heat loss. Equation (5) calculates the thermal conductivity after knowing the (e) value. The results are shown in Table 2.

The thermal conductivity (k) of the blended polymers of PAA-PVA showed higher results than PAAm-PVA. The contribution of graphene oxide exhibited significant improvement in both nanocomposites. PAA-PVA/GO revealed the best thermal conductivity (K) compared to all samples. The effect of the polymer functional group showed notable improvement of the thermal conductivity up to 67.1% of PAA-PVA/GO with the contribution of GO compared with PAAm-PVA/GO. These results supported the TGA finding that demonstrated strongly affected thermal degradation of PAA-PVA/GO. In contrast, PAAm-PVA/GO exhibited higher thermal stability with the change of temperature up to 900 °C.

Table 2 The thermal conductivity of blended polymers and nanocomposites

Sample	T (ºC)	d *10^{-3} (m)	E (W/m^2 ºC)	K (W/m ºC)
PAA-PVA	T_1 = 47 T_2 = 48 T_3 = 48	d_1 = 0.2 d_2 = 0.21 d_3 = 0.23	8.18	10.76
PAA-PVA/GO	T_1 = 36 T_2 = 36.5 T_3 = 36,5	d_1 = 0.2 d_2 = 0.21 d_3 = 0.21	8.44	16.249
PAAm-PVA	T_1 = 43 T_2 = 46 T_3 = 46	d_1 = 0.6 d_2 = 0.61 d_3 = 0.61	8.62	3.54
PAAm-PVA/GO	T_1 = 49 T_2 = 50 T_3 = 50	d_1 = 0.6 d_2 = 0.61 d_3 = 0.62	8.11	11.24

This finding is promising for thermal applications, where PAAm-PVA/GO could use for electronic applications that require thermal stability. In contrast, PAA-PVA/GO was strongly changed and affected under thermal degradation that could use in several applications such as thermistors and thermal sensors. Moreover, these samples showed good absorption of the mechanical ultrasound wave, indicating promising potential applications such as landfilling chemical, nuclear, and radioactive waste.

The ultrasound velocities, ultrasound absorption coefficient, compressibility, and the elastic modulus with 45 kHz frequency of the ultrasound wave were recorded in all the samples, as illustrated in Table 3. Equation (6) was used to calculate the ultrasonic velocity (V) [51].

$$V = \frac{X}{t} \quad (6)$$

where (X) and (t) are the sample's thickness and the wave's recording time across the samples, respectively. These measurements were considered from the ultrasound meter. The amplitude of the final ultrasound waves after absorption of ultrasound wave (A) through the samples in calculating the absorption coefficient (α) by applying Lambert Birkma's Law (2).

$$A = A_o exp^{(-\alpha X)} \quad (7)$$

where (A_o) means the initial amplitude of the ultrasound absorption. Compressibility (B) was calculated using the Laplace equation [52].

$$B = (\rho V^2)^{-1} \quad (8)$$

where (ρ) means the density. Equation (9) was considered to calculate the elasticity modulus (k) of samples [53].

Table 3 Summarized the ultrasound velocity, ultrasound absorption coefficient, compressibility, and the elastic modulus with 45 kHz frequency of the ultrasound wave of the samples

Samples	V ($m\ s^{-1}$)	α (m^{-1})	B ($mL\ s^2\ g^{-1}\ m^{-2}$)	k ($g\ m^2\ mL^{-1}\ s^{-2}$)
PAA-PVA	4.20	0.33	0.021	39.87
PAA-PVA/GO	7.80	0.68	0.005	126.74
PAAm-PVA	5.85	0.43	0.011	73.79
PAAm-PVA/GO	9.80	0.83	0.002	208.78

$$k = \rho V^2 \tag{9}$$

The ultrasound velocity significantly improved after incorporating GO up to 25% for PAAm-PVA compared to 30% for PAA-PVA and their nanocomposites. The absorption coefficient of the PAAm-PVA was higher up to 28.5% compared to PAA-PVA. It increased after incorporating GO into PAAm-PVA/GO up to 21.4% compared to the PAA-PVA/GO nanocomposites. Compared to their blended polymers, these nanocomposites were notably improved up to 100% of PAAm-PVA/GO and 89% of PAA-PVA/GO nanocomposites.

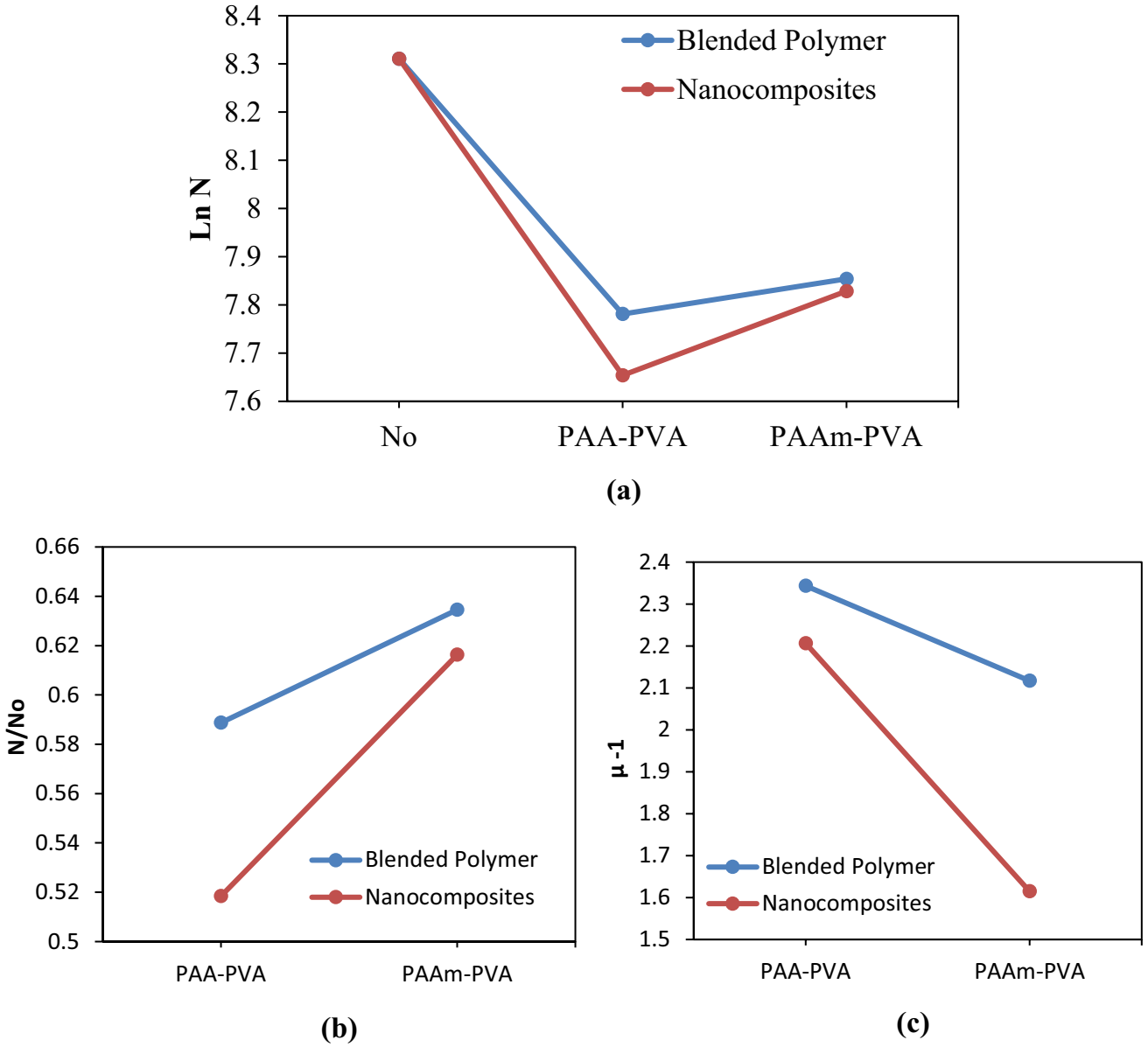

Fig. 6 (**a**) the Ln of radiation attenuation (N), (**b**) the ratio between the radiation attenuation (N) and the radiation particles number (No), and (**c**) the coefficient of radiation attenuation (μ) with samples

The results significantly improved after the addition of GO, which increased the interfacial interactions between the functional group of the polymeric chains, as exists clearly in the FTIR. However, the results of PAAm samples contained amid group higher than those PAA samples contained acid group. These results supported and behaved similarly to other researchers' findings [4, 53].

The polymer with the amide group exhibited higher results, up to 47% and 46.5% of compressibility and modulus of elasticity, respectively than the polymer with an acid group. In contrast, the compressibility value presented notable improvement after the contribution of GO up to 76% and 81%, respectively. Elasticity modulus significantly improved up to 233% of the PAA-PVA/GO and 148% of the PAAm-PVA/GO nanocomposites compared to their blended polymers, as shown in Table 3. This significant improvement is related to the strong reinforcement of nanocomposites by graphene oxide.

Radiation adsorption of the blended polymers and nanocomposites is illustrated in Fig. 6. Figure 6a and b show the Ln of radiation attenuation (N) and the ratio between the radiation attenuation (N) and the radiation particles number (No) with samples. It is noticed that PAA-PVA adsorbed a higher amount of the radiation ray compared to PAAm-PVA. Meanwhile, the contribution of graphene oxide significantly enhanced the radiation absorption in both nanocomposites. PAA-PVA/GO exhibited the best radiation adsorption among all samples, as revealed in Fig. 6.

Figure 6c shows the relationship between the coefficients of radiation attenuation (μ) and the samples. Formulation (7) was functional to estimate the ($\mu = \alpha$), the counted number ($N = A$), (x) refers to the sample thickness, and ($N_o = A_o$) is the radiation particle number. The blended polymer exhibited a good ability to absorb the radiation ray, where the involvement of GO nanosheets significantly reduced the radiation transmitter. Moreover, The PAA-PVA/GO presented the best attenuation coefficient compared with other samples. This possibility led to the absorption of the passed radiation rays through the nanocomposites that exponentially decreased up to 6% of PAA-PVA/GO and 24% of PAAm-PVA/GO nanocomposites compared to their polymers. The scattering form reduced the absorption according to Lambert law. These findings displayed a promising capacity of absorption for these nanocomposites that opens ways for wide absorbing applications [54].

Conclusions

Nanocomposites were successfully fabricated using a developed method. Nanocomposites exhibited homogeneous samples by OM and SEM images, and strong interfacial interaction formed between the components of nanocomposites as presented by FTIR and FTIR. Even though the same polymer has the same backbone, TGA spectra showed a different behaviour of each polymer due to the impact of the functional group of the polymer. After the GO contribution, the slight enhancement of the TGA reached up to 25% of PAA-PVA and 20% of PAAm-PVA. The acid group nanocomposites showed the best thermal conductivity up to 225% of the PAAm-PVA/GO nanocomposites. The best result was improved from 10.76 up to 16.24 W/m oC of PAA-PVA/GO nanocomposites. Amid group's samples demonstrated the best mechanical properties up to 100% of the PAAm-PVA/GO nanocomposites. These results show the ability to use nanocomposites as sensors for heating, smoke detectors, thermistors, etc. Nanocomposites showed a significant improvement in radiation absorption under the contribution of GO. In contrast, samples with amid group revealed better radiation absorption of up to 24% of PAAm-PVA/GO nanocomposites than samples with the acid group. According to the present results, nanocomposites show an aptitude for shielding materials for ionising radiation or west management applications.

Supplementary Information The online version contains supplementary material available at https://doi.org/10.1007/s10965-022-03210-3.

Acknowledgements The authors gratefully acknowledge the MSE at the University of Sheffield, the UK, composites. Nanomaterials group at the department of physics, the University of Babylon, Ira,q for their support.

Funding We confirmed that no fund had an applicant.

Data availability We confirm that all data and materials are authentic and available.

Declarations

Conflict of interest The authors declare that they have no conflict of interest.

References

1. Díez-Pascual AM, Gómez-Fatou MA, Ania F, Flores A (2015) Nanoindentation in polymer nanocomposites. Prog Mater Sci 67:1–94. https://doi.org/10.1016/j.pmatsci.2014.06.002
2. Al-Bermany E, Chen B (2021) Preparation and characterisation of poly(ethylene glycol)-adsorbed graphene oxide nanosheets. Polym Int 70:341–351. https://doi.org/10.1002/pi.6140
3. Layek RK, Nandi AK (2013) A review on synthesis and properties of polymer functionalized graphene. Polymer 54:5087–5103. https://doi.org/10.1016/j.polymer.2013.06.027
4. Kadhim MA, Al-Bermany E (2021) New fabricated PMMA-PVA/graphene oxide nanocomposites: Structure, optical properties and application. J Compos Mater 55:2793–2806. https://doi.org/10.1177/0021998321995912
5. Bin-Dahman OA, Shehzad F, Al-Harthi MA (2018) Influence of graphene on the non-isothermal crystallization kinetics of

poly(vinyl alcohol)/starch composite. J Polym Res 25. https://doi.org/10.1007/s10965-017-1400-7
6. Sui T, Song B, Zhang F, Yang Q (2016) Effects of functional groups on the tribological properties of hairy silica nanoparticles as an additive to polyalphaolefin. Royal Soc Chem 6:393–402. https://doi.org/10.1039/c5ra22932d
7. Fu K, Lü F, Xie Q et al (2020) The effects of shape and mass fraction of nano-SiO2 on thermomechanical properties of nano-SiO2/DGEBA/MTHPA composites: A molecular dynamics simulation study. AIP Adv 10:1–9. https://doi.org/10.1063/1.5135627
8. Parvin N, Babapoor A, Nematollahzadeh A, Mousavi SM (2020) Removal of phenol and β-naphthol from aqueous solution by decorated graphene oxide with magnetic iron for modified polyrhodanine as nanocomposite adsorbents: Kinetic, equilibrium and thermodynamic studies. React Funct Polym 156:104718. https://doi.org/10.1016/j.reactfunctpolym.2020.104718
9. Lee C, Wei X, Kysar JW, Hone J (2008) Measurement of the Elastic Properties and Intrinsic Strength of Monolayer Graphene. Science 321:385–388. https://doi.org/10.1126/science.1159499
10. Li XS, Zhu YW, Cai WW et al (2009) Transfer of Large-Area Graphene Films for High-Performance Transparent Conductive Electrodes. Nano Lett 9:4359–4363. https://doi.org/10.1021/nl902623y
11. Abdul kadhim M, Al-bermany E (2020) Enhance the Electrical Properties of the Novel Fabricated PMMA-PVA/ Graphene Based Nanocomposites. J Green Eng 10:3465–3483
12. Zhang S, Liu P, Zhao X, Xu J (2018) Enhanced tensile strength and initial modulus of poly(vinyl alcohol)/graphene oxide composite fibers via blending poly(vinyl alcohol) with poly(vinyl alcohol)-grafted graphene oxide. J Polym Res 25. https://doi.org/10.1007/s10965-018-1471-0
13. Chen J, Yao B, Li C, Shi G (2013) An improved Hummers method for eco-friendly synthesis of graphene oxide. Carbon 64:225–229. https://doi.org/10.1016/j.carbon.2013.07.055
14. Al-Abbas SS, Ghazi RA, Al-shammari AK et al (2021) Influence of the polymer molecular weights on the electrical properties of Poly(vinyl alcohol) – Poly(ethylene glycols)/Graphene oxide nanocomposites. Mater Today: Proc 42:2469–2474. https://doi.org/10.1016/j.matpr.2020.12.565
15. Bhattacharya M (2016) Polymer nanocomposites-A comparison between carbon nanotubes, graphene, and clay as nanofillers. Materials 9:1–35. https://doi.org/10.3390/ma9040262
16. Kim H, Abdala AA, MacOsko CW (2010) Graphene/polymer nanocomposites. Macromolecules 43:6515–6530. https://doi.org/10.1021/ma100572e
17. Raza Y, Raza H, Ahmad A et al (2021) Production and investigation of mechanical properties of graphene/polystyrene nano composites. J Polym Res 28:217. https://doi.org/10.1007/s10965-021-02560-8
18. Hou L, Gao J, Ruan H et al (2020) Correction to: Mechanical and thermal properties of hyperbranched poly(ε-caprolactone) modified graphene/epoxy composites. J Polym Res 27:146. https://doi.org/10.1007/s10965-020-02044-1
19. Lago E, Toth PS, Pugliese G et al (2016) Solution blending preparation of polycarbonate/graphene composite: Boosting the mechanical and electrical properties. RSC Adv 6:97931–97940. https://doi.org/10.1039/c6ra21962d
20. Noh YJ, Joh HI, Yu J et al (2015) Ultra-high dispersion of graphene in polymer composite via solvent free fabrication and functionalization. Sci Rep 5:1–7. https://doi.org/10.1038/srep09141
21. Du J, Cheng HM (2012) The fabrication, properties, and uses of graphene/polymer composites. Macromol Chem Phys 213:1060–1077. https://doi.org/10.1002/macp.201200029
22. Lavoratti A, Zattera AJ, Amico SC (2019) Mechanical and dynamic-mechanical properties of silanized graphene oxide/epoxy composites. J Polym Res 26. https://doi.org/10.1007/s10965-019-1805-6
23. Massoud A, Farid OM, Maree RM et al (2020) An improved metal cation capture on polymer with graphene oxide synthesized by gamma radiation. React Funct Polym 151. https://doi.org/10.1016/j.reactfunctpolym.2020.104564
24. Jo H, Sim M, Kim S et al (2017) Electrically conductive graphene/polyacrylamide hydrogels produced by mild chemical reduction for enhanced myoblast growth and differentiation. Acta Biomater 48:100–109. https://doi.org/10.1016/j.actbio.2016.10.035
25. Billmeyer FW (1963) Textbook of Polymer Science. Kobunshi 12:240–251. https://doi.org/10.1295/kobunshi.12.240
26. Aldulaimi NR, Al-Bermany E (2021) New Fabricated UHMWPEO-PVA Hybrid Nanocomposites Reinforced by GO Nanosheets: Structure and DC Electrical Behaviour. J Phys: Conf Ser 1973:012164. https://doi.org/10.1088/1742-6596/1973/1/012164
27. Badawi A, Mersal GAM, Shaltout AA et al (2021) Exploring the structural and optical properties of FeS filled graphene/PVA blend for environmental-friendly applications. J Polym Res 28:1–12. https://doi.org/10.1007/s10965-021-02626-7
28. Saeed AA, Balwa BD (2016) Structural and AC Electrical Properties of (LDPE-MWCNTs) Polymer Nanocomposite. Mustansiriyah J Sci Educ 17:49–62
29. Lu YJ, Yang HW, Hung SC et al (2012) Improving thermal stability and efficacy of BCNU in treating glioma cells using PAA-functionalized graphene oxide. Int J Nanomed 7:1737–1747. https://doi.org/10.2147/IJN.S29376
30. Osma B, Evingür GA, Pekcan Ö (2019) Effect of temperature and graphene oxide on the swelling of PAAm-GO composite gels. Proc World Cong New Technol 0:6–10. https://doi.org/10.11159/icnfa19.146
31. Li T, Li Y, Wang X et al (2019) Thermally and Near-Infrared Light-Induced Shape Memory Polymers Capable of Healing Mechanical Damage and Fatigued Shape Memory Function. ACS Appl Mater Interfaces 11:9470–9477. https://doi.org/10.1021/acsami.8b21970
32. Yue YM, Xu K, Liu XG et al (2008) Preparation and characterization of interpenetration polymer network films based on poly(vinyl alcohol) and poly(acrylic acid) for drug delivery. J Appl Polym Sci 108:3836–3842. https://doi.org/10.1002/app.28023
33. Shen J, Yan B, Li T et al (2012) Study on graphene-oxide-based polyacrylamide composite hydrogels. Compos A Appl Sci Manuf 43:1476–1481. https://doi.org/10.1016/j.compositesa.2012.04.006
34. Deshmukh K, Ahmad J, Hägg MB (2014) Fabrication and characterization of polymer blends consisting of cationic polyallylamine and anionic polyvinyl alcohol. Ionics 20:957–967. https://doi.org/10.1007/s11581-013-1062-3
35. Abdelamir AI, Al-Bermany E, Sh Hashim F (2019) Enhance the Optical Properties of the Synthesis PEG/Graphene- Based Nanocomposite films using GO nanosheets. J Phys: Conf Ser 1294:022029. https://doi.org/10.1088/1742-6596/1294/2/022029
36. Wang X, Li X, Zheng G et al (2006) In situ synthesis of PVA-PAA-HA interpenetrating composite hydrogel. In: Key Eng Mater. pp 1165–1168. https://doi.org/10.4028/www.scientific.net/KEM.309-311.1165
37. Guo R, Jiao T, Xing R et al (2017) Hierarchical AuNPs-Loaded Fe3O4/Polymers Nanocomposites Constructed by Electrospinning with Enhanced and Magnetically Recyclable Catalytic Capacities. Nanomaterials 7:317. https://doi.org/10.3390/nano7100317
38. Liu T, Jiao C, Peng X et al (2018) Super-strong and tough poly(vinyl alcohol)/poly(acrylic acid) hydrogels reinforced by hydrogen bonding. J Mater Chem B 6:8105–8114. https://doi.org/10.1039/c8tb02556h
39. Rajesh K, Crasta V, Rithin Kumar NB et al (2019) Structural, optical, mechanical and dielectric properties of titanium dioxide doped PVA/PVP nanocomposite. J Polym Res 26. https://doi.org/10.1007/s10965-019-1762-0

40. El-Gamal S, El Sayed AM (2019) Physical properties of the organic polymeric blend (PVA/PAM) modified with MgO nanofillers. J Compos Mater 53:2831–2847. https://doi.org/10.1177/0021998319840802
41. Yang CC (2004) Chemical composition and XRD analyses for alkaline composite PVA polymer electrolyte. Mater Lett 58:33–38. https://doi.org/10.1016/S0167-577X(03)00409-9
42. Yang Z, Zhang Y, Wen B (2019) Enhanced electromagnetic interference shielding capability in bamboo fiber@polyaniline composites through microwave reflection cavity design. Compos Sci Technol 178:41–49. https://doi.org/10.1016/j.compscitech.2019.04.023
43. Qiu M, Zhang Y, Wen B (2018) Facile synthesis of polyaniline nanostructures with effective electromagnetic interference shielding performance. J Mater Sci: Mater Electron 29:10437–10444. https://doi.org/10.1007/s10854-018-9100-6
44. Chen Y, Qi Y, Liu B (2013) Polyacrylic acid functionalized nanographene as a nanocarrier for loading and controlled release of doxorubicin hydrochloride. J Nanomater 2013:1–8. https://doi.org/10.1155/2013/345738
45. Zhong Y, Huang LH, Sen ZZ et al (2016) Enhancing the specificity of polymerase chain reaction by graphene oxide through surface modification: Zwitterionic polymer is superior to other polymers with different charges. Int J Nanomed 11:5989–6002. https://doi.org/10.2147/IJN.S120659
46. Lim BC, Singu BS, Hong SE et al (2016) Synthesis and characterization nanocomposite of polyacrylamide-rGO-Ag-PEDOT/PSS hydrogels by photo polymerization method. Polym Adv Technol 27:366–373. https://doi.org/10.1002/pat.3648
47. Dweik H, Sultan W, Sowwan M, Makharza S (2008) Analysis characterization and some properties of polyacrylamide copper complexes. Int J Polym Mater Polym Biomater 57:228–244. https://doi.org/10.1080/00914030701413280
48. Wan C, Chen B (2012) Reinforcement and interphase of polymer/graphene oxide nanocomposites. J Mater Chem 22:3637. https://doi.org/10.1039/c2jm15062j
49. Lees CH, Chorlton JD (1896) LIV. On a simple apparatus for determining the thermal conductivities of cements and other substances used in the arts. The London Edinburgh Dublin Philosophic Magz J Sci 41:495–503. https://doi.org/10.1080/14786449608620875
50. Majeed NS, Salih SM, Abdulmajeed BA (2019) Effect of nanoparticles on thermal conductivity of epoxy resin system. IOP Conf Ser: Mater Sci Eng 518. https://doi.org/10.1088/1757-899X/518/6/062006
51. Classic K (2002) Medical Imaging Physics, Fourth Edition. Health Phys 83:921. https://doi.org/10.1097/00004032-200212000-00023
52. Rashid A-KJ, Jawad ED, Kadem BY (2011) A Study of Some Mechanical Properties of Iraqi Palm Fiber-PVA Composite by Ultrasonic. Eur J Sci Res 61:203–209
53. Abdelamir AI, Al-Bermany E, Hashim FS (2020) Important factors affecting the microstructure and mechanical properties of PEG/GO-based nanographene composites fabricated applying assembly-acoustic method. In: AIP Conference Proceedings. p 020110. https://doi.org/10.1063/5.0000175
54. AttaM Madbouly ERZKAM (2015) Study on Polymer Clay Layered Nanocomposites As Shielding Materials for Ionizing Radiation. Int J Recent Sci Res 6:4263–4269